# Journal of Materials Chemistry

**PAPER**

# Dewetting of Au nanoparticle assemblies

**Haya Alhummiany, Samuel Jarvis, Richard A. J. Woolley, Andrew Stannard, Matthew Blunt†
and Philip Moriarty***

Atomic force microscopy measurements as a function of annealing temperature, time of exposure to a high relative humidity environment, and scan duration/parameters have been used to ascertain the stability of assemblies of thiol-passivated Au nanoparticles on silicon substrates. Striking changes in the morphology of self-organised nanoparticle patterns are observed following the exposure of samples to atmospheres with a relative humidity of 80%. The nanoparticle film dewets the underlying silicon substrate on exposure to water, forming locally thicker regions. Time-lapse imaging shows that the dewetting proceeds *via* layer-by-layer growth, and there is no evidence for classical coarsening mechanisms involving self-similar film morphologies. Annealing at temperatures between 100 °C and 160 °C produces a rather different dewetting effect for the highest temperatures and/or annealing times, where significant nanoparticle sintering promotes the break-up of the two-dimensional assembly. The morphology of the initial 2D film plays a key role in determining the time scale on which annealing promotes nanoparticle dewetting. Dewetting can also be induced by a scanning probe such that localised (micron-scale) areas of the nanoparticle assembly can be converted from 2D to 3D character.

## 1. Introduction

Deposition of colloidal nanoparticles from organic solvents onto solid substrates results in a fascinating and diverse array of self-organised patterns.[1] The majority of these patterns, which include cellular networks,[2,3] spinodal "worms" and labyrinths,[4–7] rings, lines, and concentric circles,[8–14] and branched/fingered structures,[9,15,16] are non-equilibrium structures which are "frozen" in place due to rapid solvent evaporation. As described in detail by Rabani *et al.*,[5] the coupling of solvent and nanoparticle dynamics opens up a rich parameter space whereby the evaporative and/or convective dewetting of the solvent "imprints" a particular type of nanoparticle pattern.

In addition to representing an important archetypal system and "playground" in which to study the dynamics of self-assembly and self-organisation, the formation and stability of nanoparticle arrays is of particular importance for nano-electronic device architectures. Extending the seminal work of Middleton and Wingreen in the early nineties,[17] Parthasarathy *et al.*[18,19] have carefully analysed the transport characteristics of highly ordered 2D superlattices of gold nanoparticles. They found that the Couloumb-blockade-mediated tunnelling process that underpins charge transport through 2D arrays of thiol-passivated Au nanoparticles gives rise to power law I(V)

behaviour (above a certain threshold voltage). The power law exponent is directly related to the degree of structural order in the lattice and for sufficiently high levels of disorder, a single power law is no longer sufficient to describe the current–voltage behaviour. Exponents as high as 4 have been observed for topologically complex 2D nanoparticle assemblies formed *via* various solvent dewetting mechanisms.[20]

As nanoparticle-based materials become increasingly important in technology - it has been claimed, for example, that next-generation touch screens will exploit pressure-induced changes in the conductivity of a nanoparticle-elastomer hybrid material[21] - the stability of nanostructured assemblies against changes in temperature and operating environment is a key issue to address. Important work in this area has been carried out by a number of groups, although there has perhaps been less focus on the thermal/environmental stability of nanoparticle arrays than one might at first expect. A decade ago, Sandhyarani *et al.*[22] found that superlattices of thiol-passivated Ag nanoparticles were stable up to a temperature of 100 °C. Above this temperature the superlattice melted, with differential scanning calorimetry showing two transitions: melting of the alkyl chains followed by melting of the superlattice. Korgel[23] subsequently showed that Ag nanoparticle superlattices exhibited a power law dependence of the extent of spatial disorder as a function of annealing temperature and that *correlated* fluctuations of the passivating ligands underpinned the temperature dependence of the lattice. Using a capacitance bridge method to "non-invasively" detect the conductivity of a nanoparticle film, Martin *et al.*[24] demonstrated that 6 nm diameter alkanethiol-capped Au

*School of Physics and Astronomy, University of Nottingham, Nottingham, NG7 2RD, United Kingdom. E-mail: philip.moriarty@nottingham.ac.uk*
† Now at the Scanning Probe Microscopy Group, Laboratory of Photochemistry and Spectroscopy, Department of Chemistry, KU Leuven, Celestijnenlaan 200F, B-3001 Heverlee, Belgium.

This journal is © The Royal Society of Chemistry 2011

*J. Mater. Chem.*, 2011, **21**, 16983–16989 | 16983

nanoparticle films sintered at a temperature close to 210 °C. Remarkably, Martin et al. found no dependence of the sintering temperature on the size of the nanoparticles - 2.0 nm particle films sintered at the same temperature as 6.0 nm diameter nanoparticle films. Moreover, and perhaps counter-intuitively, sintering was found not to be driven by thiol desorption - films sintered with little loss of thiol. Indeed, for octanethiol, thiol desorption was driven by sintering of the nanoparticles, instead of the other way round. Annealing has also been shown to dramatically influence the electronic properties of CoPt$_3$ nanoparticle superlattices, driving an insulator-to-metal transition.[25]

Most recently, Lin's group at Argonne National Lab. has used grazing incidence X-ray diffraction to study the thermal stability of 2D assemblies of thiol-passivated gold nanoparticles.[26,27] They found significant differences between the behaviour of the assemblies when annealed under a vacuum, as compared to heating in air, and interpreted their results in terms of the differences in evaporation rate of the thiol molecules in vacuum as compared to in air. Sintering occurred at temperatures > 100 °C in vacuum and at > 160 °C in air (following prolonged heating for periods of several hours for the latter). Robel et al. also highlighted the important contribution of excess thiol molecules to the temperature-dependent behaviour of Au nanoparticle super lattices. Their results contrasted with the observations of Santiago et al.[28] for three-dimensional thiol-passivated Au nanoparticle assemblies where annealing at temperatures up to 275 °C produced little, if any, discernable change in the structure or order of the superlattice.

Here we complement those recent reciprocal space (X-ray diffraction) studies of the stability of nanoparticle assemblies with real space (atomic force microscopy (AFM)) analyses of the effects of not only annealing but exposure to high relative humidity environments and relatively strong tip–nanoparticle interactions during AFM scanning. In each case the nanoparticle assembly in essence dewets the underlying native oxide-terminated silicon substrate, leading to the formation of three dimensional islands whose height (i.e. thickness) is much greater than that of the starting film, in a manner qualitatively reminiscent - in terms of the resulting mesoscopic morphology at least - of the dewetting of thin films on solid substrates to form quantum dots. The dewetting process for the nanoparticle assemblies studied here is, however, significantly complicated by the sintering of nanoparticles during thermal annealing and the presence of thiol surfactant both bound to the nanoparticles and free on the substrate surface. Our results provide important insights into the morphological changes that can be driven by changes in the environment of nanoparticle assemblies and are significant in terms of characterising the longevity of nano-electronic devices based on Coloumb-blockade mediated transport in these systems.

## 2. Experimental

We used ~2 nm core-size octanethiol-passivated Au nanoparticles, synthesised via the Brust et al. technique,[29] and dispersed in one of a number of solvents (toluene, hexane, chloroform, or dichloromethane) at a concentration of ~ 1 mg ml$^{-1}$. A 25 µl droplet of this solution was deposited onto a $1 \times 1$ cm$^2$ square piece of a native oxide-terminated, and solvent cleaned, Si(111) substrate and spin-coated at 4,000 r.p.m. to produce a uniform thin film which subsequently thins though evaporative loss of solvent.

Atomic force microscopy imaging was carried out using an Asylum Research MFP-3D system operating in either tapping mode (TM) or non-contact mode (i.e. where the tip–sample interaction remains in the attractive regime throughout the entire tip oscillation cycle). For the humidity-related studies, the AFM was operated in a closed environment where the relative humidity could be increased to a maximum of ~ 85%. Asylum Research's CoolerHeater Peltier stage for the MFP-3D system was used to heat samples in situ, although samples were also annealed in an oven and returned to the AFM for analysis.

## 3. Results and discussion

### 3.1. Humidity

We have recently demonstrated that adsorbed water can play a very significant role in determining the morphology of Au nanoparticle films which have been produced by spin-casting from an organic solvent.[14] In particular, the condensation of water droplets via the so-called "breath figure" process,[30,31] leads to the templating of nanoparticle rings. John et al.[32] have also convincingly shown that water adsorption under high humidity conditions plays a central role in the organisation of gold nanoparticles on mica (a hydrophilic substrate). In particular, they attribute the formation of nanoparticle networks on mica to the nucleation and growth of water islands.

Here we are interested in the influence of adsorbed water on the nanoparticle film formed following the spin coating process. As an initial experiment we simply took a thin film formed from octanethiol-passivated nanoparticles and spin cast a droplet of de-ionised water onto the surface of the sample. Fig. 1(a) is a representative image of the nanoparticle assembly prior to water deposition. Note that the majority of the sample is covered with flat, quasi-2D regions, between 5 nm and 6 nm in height, although there are some areas which are higher due to the formation of a locally thicker film. (It is worth noting at this point that there can be significant differences between the value of the height of a nanoparticle layer measured by NC-AFM and that expected on the basis of the value of the Au core diameter-plus-ligand chain length.[33,34,35] We return to a discussion of this point below in the context of Fig. 7.). Deposition of a water droplet produced the morphology shown in Fig. 1(b). Although this is a different region of the sample surface as compared to that shown in Fig. 1(a), the changes are representative of the entire sample surface: the deposition of water leads to a conversion of the largely flat "quasi-2D" nanoparticle islands into 3D aggregates.

The results of a rather more controlled experiment are shown in Fig. 2. In this case, the same region of a nanoparticle assembly was scanned by AFM under a relative humidity of 80% at hourly intervals for a total duration of 24 h, enabling the evolution of the surface morphology to be followed in real time. From the images shown in Fig. 2(a)-(c) it is clear that the high relative humidity environment promotes the formation of three-dimensional nanoparticle aggregates at the expense of the flat areas, similar to the results of the droplet experiment shown in Fig. 1.
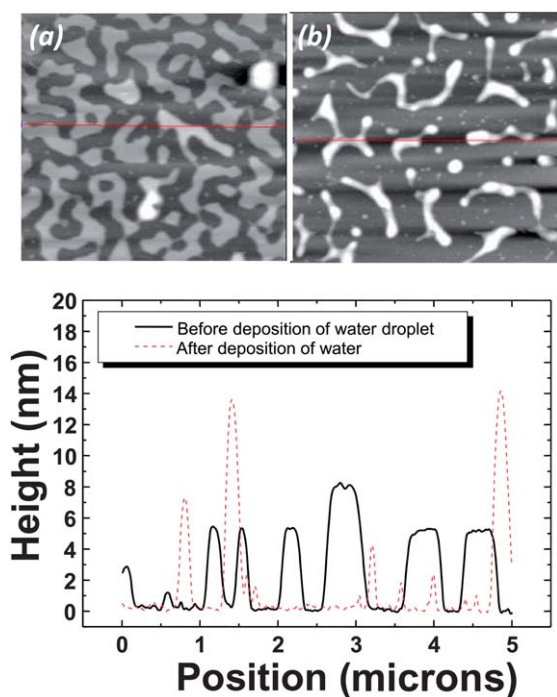
**Fig. 1** Tapping mode atomic force microscope images ($5 \times 5$ µm$^2$) of a self-organised nanoparticle film on a silicon substrate, (a) before, and (b) after the deposition of a deionised water droplet on the surface. (The same surface area is not shown in each case but the images are representative of the morphology across the sample surface.) Line profiles are shown below the images to illustrate that the average height of the nanoparticle islands changes significantly following the deposition of water - the assembly of (largely) flat islands shown in (a) dewets to form much higher 3D aggregates.



**Fig. 2** Time-lapse AFM imaging of dewetting of a nanoparticle assembly. Images (a), (b), and (c) (each $5 \times 5$ µm$^2$) were taken after 0, 12, and 24 h exposure of the sample to an atmosphere of 80% relatively humidity. The arrows in (a) point to nanoparticle features which are eroded by the presence of water (and whose constituent particles are redeposited in higher layers) while the circle highlights a nanoparticle island that remains unchanged throughout the period of exposure to water and thus acts as a marker. The images shown in (d) and (e) are larger scale ($20 \times 20$ µm$^2$) and show that the AFM tip in this case does not drive the dewetting process in the repeatedly scanned area (highlighted by a yellow square in each image).

In order to quantify, to some extent, the kinetics of the dewetting process, we have plotted the change in the total area of the uncovered (*i.e.* nanoparticle-free) silicon substrate as a function

Unlike Fig. 1, however, the real time study of Fig. 2 enables the evolution of the tall 3D islands to be followed, indicating very clearly that these nanoparticle aggregates form *via* layer-by-layer growth in this case. It is important to note that, as shown previously[6] and described in more detail below, the AFM tip can itself drive an Ostwald ripening-like coarsening of nanoparticle assemblies under certain experimental conditions. To ensure that the probe was not driving or accelerating the evolution of the nanoparticle film we acquired a single image of a $20 \times 20$ µm$^2$ area surrounding the smaller ($5 \times 5$ µm$^2$) repeatedly scanned region both at the start and at the end of the 24 h period. The corresponding images are shown in Fig. 2(d) and (e) where accelerated dewetting due to the probe is not observed in the repeatedly scanned area (highlighted by a square in the images).

The larger area images are also useful for the calculation of relatively low noise and representative radially-averaged 2D Fourier transforms. We have previously shown that probe-induced coarsening of 2D nanoparticle assemblies produces self-similar morphologies (as evidenced by our ability to collapse radially averaged Fourier transforms of AFM images onto a single master curve[6]). Unlike the case for probe-induced coarsening, the transforms for images 2(d) and 2(e) cannot be collapsed onto a master function (not shown). Humidity-driven dewetting proceeds in this case by the erosion of the initial extended "worm-like" morphology to form isolated 3D islands.
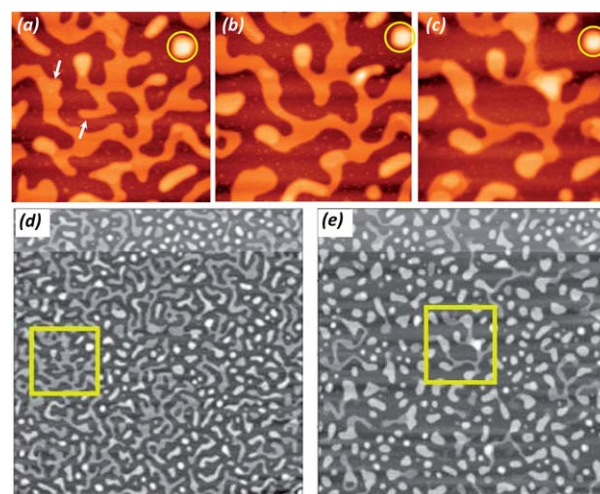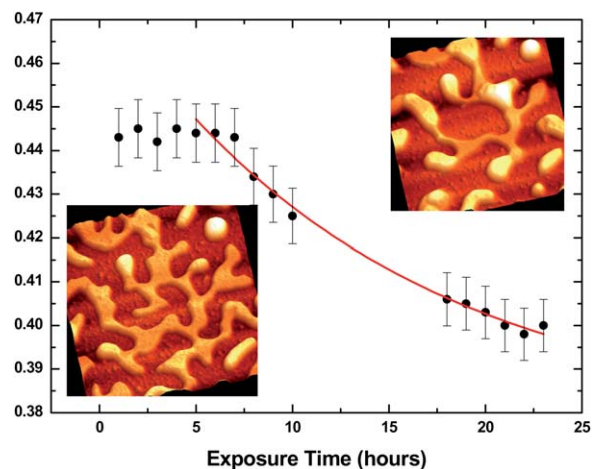


**Fig. 3** Fractional area of the sample surface covered by nanoparticles as a function of the time of exposure to an 80% relative humidity atmosphere. Disregarding the initial "transient" behaviour up to five hours, the remainder of the data can be fit with a simple exponential decay function (eqn (1)). The gap in the data appears because the experiment was run over the course of a 24 h period with an AFM image taken every hour (followed by the retraction of the tip a small amount from the surface). The same surface area was scanned repeatedly. The insets are $5 \times 5$ µm$^2$ images showing representative "snapshots" of the state of the surface during the dewetting process.

of time (Fig. 3). Following an initial period (up to ~ 5 h) during which there is no detectable change in the morphology of the nanoparticle assembly, there is an exponentially decreasing fraction of the silicon substrate which is covered with nanoparticles. (The eight hour period for which no data are displayed on the graph arises because the experiment was run over two days - an image was taken every hour (with the tip retracted a small distance from the surface between images)).

If we disregard the initial "transient" behaviour (up to approximately 5 h) during which the morphology of the nanoparticle assembly does not change, a simple exponential decay function provides an adequate fit to the remaining data shown in Fig. 3,

$$A(t) = A_0 e^{-t/\tau} \tag{1}$$

where $A(t)$ is the fractional area of the surface that is covered with nanoparticles at time $t$, $A_0$ is the initial fractional covered area, and $\tau$ is a decay constant.

This functional behaviour is common to very many systems including, as pointed out by Topple and co-workers, biological growth.[36] Dewetting molecular films on NaCl[36,37] and silicon[38] substrates have been shown to follow a similar evolution. The behaviour can be straight-forwardly understood in the context of the simple differential equation of which eqn (1) is a solution; as the average size of dewetting islands (or particles in general) increases, the growth rate of the system slows because the higher islands are "fed" by molecules from the surrounding ("quasi 2D") interconnected regions and there is a fixed number of particles available. We speculate that the lack of change in the morphology of the nanoparticle film up to five hours' exposure time may possibly arise from a kinetic barrier associated with the penetration of adsorbed water into the particle assembly. Temperature-dependent studies (under a high relative humidity environment) would help to clarify the origin of the "dead time" in the early stage of exposure to water vapour.

That thiol-passivated Au nanoparticles should dewet the substrate on exposure to water is not, in itself, too surprising - the thiol layer is strongly hydrophobic. What is perhaps more interesting about the results of Fig. 2 and Fig. 3 is that they show that the dewetting of the nanoparticle assemblies proceeds on a layer-by-layer basis in a manner comparable to that observed for molecular thin films. Moreover, and as discussed in the following section, in the absence of water a very different dewetting behaviour is observed. Our results strongly suggest that adsorbed water significantly lowers the effective diffusion barrier for nanoparticles on silicon substrates.

### 3.2. Annealing

The response of morphologically similar nanoparticle assemblies to annealing and to exposure to high humidity environments is dramatically different. Fig. 4(a) and 4(b) show the effect of annealing an octanethiol-passivated nanoparticle assembly, with a starting morphology quite similar to that of the sample shown in Fig. 2, to a temperature of 120 °C for ten hours. Unlike the sample that was exposed to a high relative humidity, the nanoparticle film does not dewet from the surface - islands whose height is greater than the thickness of the starting film are not
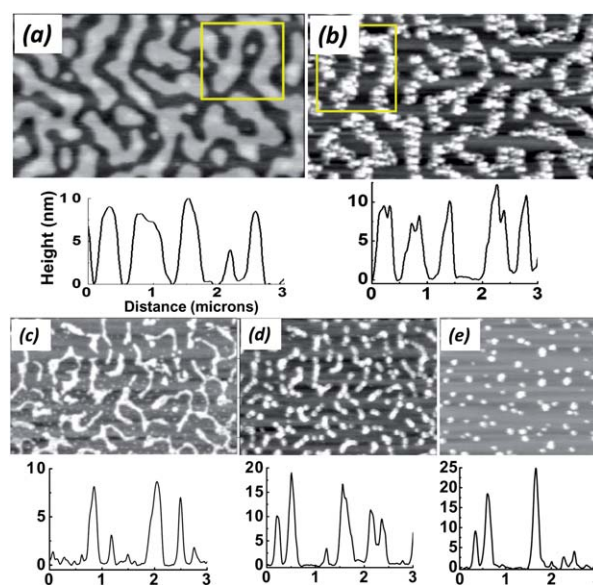


**Fig. 4** (a) "Spinodal"-type nanoparticle pattern prepared by rapid solvent evaporation ($5 \times 5$ μm$^2$ image). The width of the nanoparticle branches is relatively large in this case. The graph under the image is a representative line profile spanning 3 microns where the $y$-axis spans a 0–10 nm range. All other graphs in this figure are of the same height (nm) vs. distance (microns) form. (b) Following annealing at 120 °C for ten hours (using the heater stage incorporated in the AFM system), the film has sintered leading to a rougher film. A line profile (inset) shows, however, that the overall height of the film is very similar to that of the nanoparticle assembly shown in (a). Yellow squares in (a) and (b) show same area of surface, providing a measure of thermal drift during the imaging process. (c)-(e) A nanoparticle film with a much thinner branch width (and a less interconnected morphology) dewets much more rapidly. After three hours total anneal time (again using the AFM heater) the sample has already started to dewet, Fig. 4(d). After nine hours (Fig. 4(e), there is little evidence of the starting morphology visible in AFM images. The profiles underneath images (c)-(e) show how the height of the nanoparticle aggregates changes during the annealing process. (Image sizes for (c)-(e) are ~ $5 \times 2.5$ μm$^2$, $5 \times 2.5$ μm$^2$, and $3 \times 2.5$ μm$^2$, respectively).

observed (see line profiles accompanying the images in Fig. 4). Instead, the film becomes substantially rougher due to the sintering of nanoparticles at elevated temperatures.

Robel et al.[27] found that when Au nanoparticle samples were heated in air they retained lattice order for short periods of time at temperatures as high as 160 °C (albeit with a larger particle size (~ 6 nm) than that used in this study). Extended annealing at this temperature in air (or at lower annealing temperatures in vacuum) led to the disordering of the nanoparticle lattice.

Robel et al.'s experiments focussed on extremely well-ordered samples which exhibited long-range 2D crystallinity over many hundreds of nanometres. In our case we are interested in the role that the initial morphology of a nanoparticle assembly plays in both sintering and solid-on-solid dewetting phenomena. Solvent (as opposed to nanoparticle) dewetting pathways and kinetics have a very strong influence on the initial structure that a nanoparticle overlayer can form. That this self-organised morphology can in turn dramatically affect the stability of the overall nanoparticle assembly is clear from a comparison of Fig. 4(a) and 4(b) with Fig. 4(c)-4(e). The relatively high degree of interconnectivity

and the wide branches of the "spinodal" structure seen in Fig. 4 (a) produce more highly coordinated nanoparticles on average. Although the nanoparticles are clearly subject to significant sintering, the initial morphology significantly delays the onset of particle "dewetting" (*i.e.* the formation of 3D structures) such that even after ten hours of annealing at a temperature of 120 °C the overall structural "signature" of the original morphology is preserved. For a starting morphology with significantly thinner branches (Fig. 4(c)), dewetting of the nanoparticle film initiates at much shorter annealing periods (Fig. 4(d)). Annealing this sample at 120° for a period of nine hours (Fig. 4(e)) removes any evidence of the initial morphology of the nanoparticle assembly - the nanoparticles have formed islands up to 20 nm in height sparsely distributed across the surface.

As demonstrated by Robel *et al.*, annealing under vacuum significantly accelerates the disordering of a nanoparticle lattice. We find that even for annealing in air, the sintering and dewetting timescales can differ dramatically depending on the system used to heat the samples. We observe an acceleration of the sintering process for samples annealed in an oven as compared to those heated *in situ* in the AFM. As Martin *et al.*[24] pointed out almost a decade ago, sintering is of course a kinetically driven/limited process. It is likely that the different heating rates for the oven and the AFM heater significantly affect the extent to which nanoparticles sinter. Fig. 5 shows the evolution of a nanoparticle film annealed at 100 °C over the course of an hour. (Unlike Fig. 4, the same surface region is not shown in each image. For
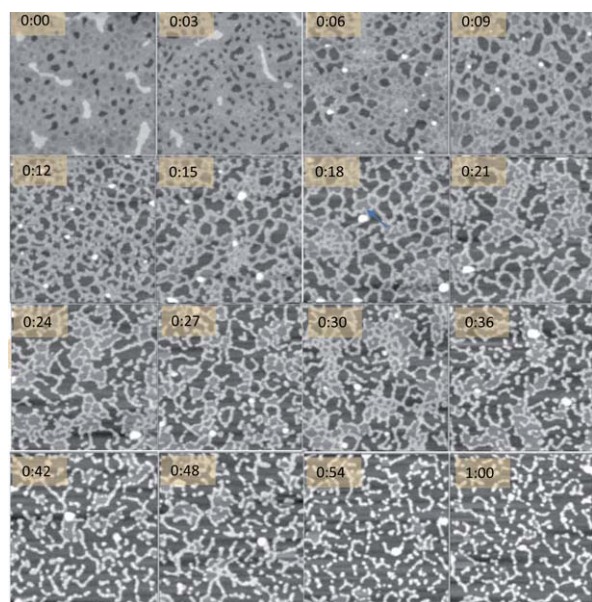
this experiment, the sample was taken back and forth to the oven and so relocation of precisely the same area was not possible). Not only do the sintering and dewetting of the nanoparticle film occur on much shorter time scales than for the sample shown in Fig.4 (significantly more than one order of magnitude faster), but Fig. 5 shows an intriguing effect we have observed for a number of samples. In addition to the break-up of the initial network and the formation of islands of aggregated nanoparticles, what is perhaps best described as an "intermediate" layer is observed throughout the sintering and dewetting process. For the majority of the images shown in Fig. 5, in addition to the contrast levels arising from the nanoparticles and the bare silicon substrate there is a layer whose contrast/apparent height falls between the two. This is most clearly observed for the images taken mid-way through the annealing process (*e.g.* those from 00:18 to 00:27 in Fig. 5) but the effect is present throughout the entire sequence.

In the absence of detailed chemical information (which might be provided either *via* scanning electron microscopy and energy dispersive X-ray analysis, or through photoelectron emission microscopy (PEEM)), we postulate that the intermediate contrast layer arises from excess thiol surfactant that is present in the solution from which the nanoparticle layer is spin-cast. It is possible that the contrast arises not from a closely packed layer but from rapidly diffusing thiol molecules. Although it initially appears as if the layer forms following annealing, this is not the case. A careful inspection of the first image in the sequence shown in Fig. 5 reveals that there are also intermediate contrast regions. That these areas comprise weakly bound adsorbates is
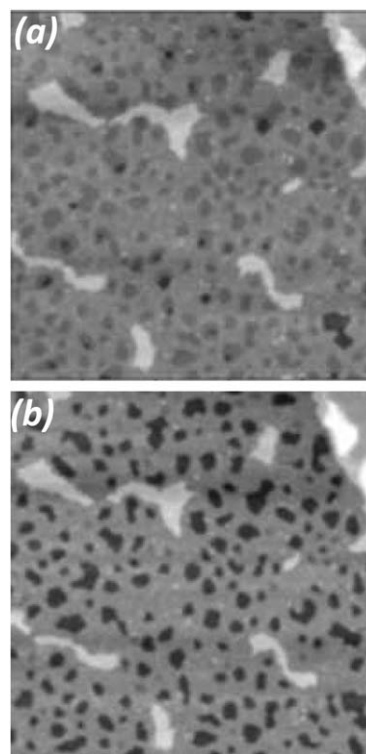


**Fig. 5** Sequence of AFM images (each 1 × 1 μm² in size) showing evolution of nanoparticle assembly as a function of annealing time at 100 °C. For this experiment the sample was annealed in an oven for a fixed period of time (either three or six minutes) and returned to the AFM to be imaged before the next heating period. Note, in particular, the presence of a layer whose apparent height is intermediate between that of the bare silicon substrate (darkest contrast region) and the nanoparticle layer (light gray). We propose that this layer arises from excess thiol surfactant which desorbs following sufficiently long annealing periods, although, as shown in Fig. 6, it is sufficiently weakly bound to be removed by the NC-AFM tip even at room temperature.



**Fig. 6** Two 1 × 1 μm² NC-AFM images of the same surface region taken after (a) one, and (b) ten scans. The "intermediate contrast" layer seen in (a), which we suggest arises from excess thiol surfactant, is removed following ten scans, revealing the bare silicon substrate.

clear from Fig. 6, two NC-AFM images taken of the same surface region following a single scan (Fig. 6(a)) and ten scans (Fig. 6(b)). Note how the intermediate contrast regions have been removed, revealing the underlying silicon substrate, in Fig. 6(b). After ten scans only a few very small intermediate contrast regions remain. The most likely explanation for the erosion of these regions is that the surfactant molecules are transferred to the tip. Note that the overall resolution is very similar in Fig. 6(a) and 6(b) so the presence (and removal) of the "intermediate contrast" layer cannot be attributed to a change in the radius of curvature of the tip (and its associated ability to probe narrow holes in the nanoparticle assembly).

### 3.3.  Tip-induced "dewetting"

In addition to the tip-induced modification of the surfactant layer, at higher tip–sample forces it is possible both to controllably coarsen a 2D nanoparticle assembly (in a fashion which mimics thermal coarsening *via* an Ostwald ripening-like mechanism[6]) and, as shown in Fig. 7, to locally drive the dewetting of the nanoparticle film. As we observed previously for 2D coarsening,[6] the tip can induce significant mass transport but, interestingly, this does not result in a "pile-up" of nanoparticles at the edges of the scan window. Instead, in the case shown in Fig. 7 the AFM tip both breaks up the 2D network and transfers nanoparticles from the first to the second layer, resulting in a final
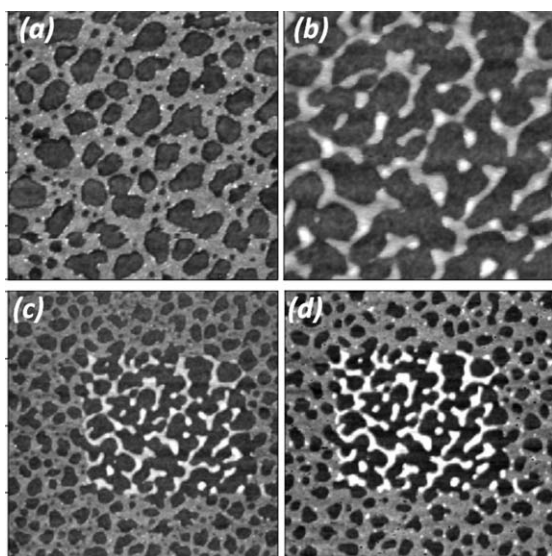


**Fig. 7**  Tip-induced dewetting of a nanoparticle assembly. (a) $1 \times 1$ μm² image taken with an amplitude setpoint chosen so as to minimise tip–sample interaction. (b) Following five scans with a higher tip–sample interaction, the 2D nanoparticle assembly has been heavily disrupted by the scanning process and 3D islands have been formed. (c) Tapping mode image (*i.e.* data acquired using by operating on the positive frequency shift side of the cantilever resonance curve) of a larger area (and with a setpoint amplitude chosen again so as to minimise the tip–sample interaction) showing the influence of the tip. (d) Non-contact image (acquired by operating on the negative frequency shift side of the resonance) of the same region as shown in (c). The average height of the nanoparticle islands for this non-contact image is approximately 50% larger than for the tapping mode data shown in (c).

morphology which is strikingly similar to that observed for both humidity-mediated and thermally-induced dewetting.

There are two interesting aspects of Fig.7 with regard to the NC-AFM imaging process. First, for scan conditions resulting in a tip–sample interaction lower than that required to promote the 3D dewetting effect seen in Fig.7, we observed the 2D coarsening effect we reported previously.[6] As the tip–sample force is increased, therefore, it appears that the barrier for the growth of 2D assemblies is first crossed before three-dimensional growth is induced. There is a clear threshold force required for the latter. Second, Fig. 7(c) and Fig. 7(d) are NC-AFM images of precisely the same surface area taken in tapping mode (*i.e.* operating on the positive frequency shift side of the resonance curve) and non-contact mode (negative frequency shift) respectively. There is a large difference in the mean height of the nanoparticle aggregates measured in the "dewetted" region for these two techniques: 6.5 nm (tapping) *vs.* 9.5 nm (non-contact). Although this "discrepancy" is not surprising - tapping mode and non-contact mode of course probe very different regions of the tip–sample interaction potential - it highlights the difficulty associated with making accurate measurements of nanoparticle height/thin film thickness with dynamic force microscopy.[33,34,35]

## 4.  Conclusions

We have studied the stability of gold nanoparticle assemblies on silicon substrates against dewetting induced *via* either a high relative humidity environment, thermal annealing, or tip–sample forces. Exposure to a high relative humidity ($\sim$ 80%) environment leads to slow dewetting over time-scales of days, with an exponential decrease in the nanoparticle-covered silicon surface area as a function of time. The humidity-driven nanoparticle dewetting phenomenon we observe has interesting parallels with the dewetting of molecular monolayers and thin films on silicon and insulating surfaces. Annealing at temperatures in excess of 100 °C leads initially to nanoparticle sintering, followed by dewetting at later stages to form isolated islands. Excess surfactant appears as small domains between the nanoparticle regions. Annealing and prolonged NC-AFM scanning both remove the surfactant layer. At high tip–sample forces, NC-AFM imaging itself promotes rapid dewetting of the nanoparticle film.

The experiments discussed in this paper have involved relatively hydrophilic, oxide-terminated silicon substrates. Future work will focus on how a modification of the surface free energy/surface chemistry *via* HF treatment, producing a hydrophobic Si(111) surface (as we have exploited in previous studies of the effects of substrate wettability on the self-organisation of Au nanoparticles[39,40]), affects the dewetting phenomena described here.

## References

1 A. Stannard, *J. Phys.: Condens. Matter*, 2011, **23**, 083001.
2 P. Moriarty, M. D. R. Taylor and M. Brust, *Phys. Rev. Lett.*, 2002, **89**, 248303.
3 C. P. Martin, M. O. Blunt and P. Moriarty, *Nano Lett.*, 2004, **4**, 2389.
4 G. Ge and L. Brus, *J. Phys. Chem. B*, 2000, **104**, 9573.
5 E. Rabani, D. R. Reichman, P. L. Geissler and L. E. Brus, *Nature*, 2003, **426**, 271.
6 M. O. Blunt, C. P. Martin, M. Ahola-Tuomi, E. Pauliac-Vaujour, P. Sharp, P. Nativo, M. Brust and P. Moriarty, *Nat. Nanotechnol.*, 2007, **2**, 167.
7 A. Stannard, C. P. Martin, E. Pauliac-Vaujour, P. Moriarty and U. Thiele, *J. Phys. Chem. C*, 2008, **112**, 15195.
8 P. C. Ohara and W. M. Gelbart, *Langmuir*, 1998, **14**, 3418.
9 G. Yosef and E. Rabani, *J. Phys. Chem. B*, 2006, **110**, 20965.
10 J. Xu, J. Xia and Z. Lin, *Angew. Chem., Int. Ed.*, 2007, **46**, 1860.
11 L. Frastia, A. J. Archer and U. Thiele, *Phys. Rev. Lett.*, 2011, **106**, 077801.
12 M. Maillard, L. Motte and M. Pileni, *Adv. Mater.*, 2001, **13**, 200.
13 A. P. H. J. Schenning, F. B. G. Benneker, H. P. M. Geurts, X. Y. Liu and R. J. M. Nolte, *J. Am. Chem. Soc.*, 1996, **118**, 8549.
14 A. Stannard, H. Alhummiany, E. Pauliac-Vaujour, J. S. Sharp, P. Moriarty and U. Thiele, *Langmuir*, 2010, **26**, 13892.
15 E. Pauliac-Vaujour, A. Stannard, C. P. Martin, M. O. Blunt, I. Notingher, P. J. Moriarty, I. Vancea and U. Thiele, *Phys. Rev. Lett.*, 2008, **100**, 176102.
16 U. Thiele, I. Vancea, A. J. Archer, M. J. Robbins, L. Frastia, A. S. E. Pauliac-Vaujour, C. P. Martin, M. O. Blunt and P. Moriarty, *J. Phys.: Condens. Matter*, 2009, **21**, 264016.
17 A. Middleton and N. S. Wingreen, *Phys. Rev. Lett.*, 1993, **71**, 3198.
18 R. Parthasarathy, X. M. Lin and H. M. Jaeger, *Phys. Rev. Lett.*, 2001, **87**, 186807.
19 R. Parthasarathy, X. M. Lin, K. Elteto, T. F. Rosenbaum and H. M. Jaeger, *Phys. Rev. Lett.*, 2004, **92**, 076801.
20 M. O. Blunt, M. Suvakov, F. Pulizzi, C. P. Martin, E. Pauliac-Vaujour, A. Stannard, A. Rushforth, B. Tadic and P. Moriarty, *Nano Lett.*, 2007, **7**, 855.
21 D. Bloor, A. Graham, E. J. Williams, P. J. Laughlin and D. Lussey, *Appl. Phys. Lett.*, 2006, **88**, 102103.
22 N. Sandhyarani, M. P. Antony, G. P. Selvam and T. Pradeep, *J. Chem. Phys.*, 2000, **113**, 9794.
23 B. A. Korgel, *Phys. Rev. Lett.*, 2001, **86**, 127.
24 J. E. Martin, J. Odinek, J. P. Wilcoxon, R. A. Anderson and P. Provencio, *J. Phys. Chem.*, 2003, **107**, 430.
25 P. Beecher, A. J. Quinn, E. V. Shevchenko, H. Weller and G. Redmond, *Nano Lett.*, 2004, **4**, 1289.
26 M. G. Constantinides, H. M. Jaeger, X. Li, J. Wang and X. M. Lin, *Z. Kristallogr.*, 2007, **222**, 595.
27 I. Robel, X. M. Lin, M. Sprung and J. Wang, *J. Phys.: Condens. Matter*, 2009, **21**, 264011.
28 P. Santiago, H. E. Troiani, C. Gutierrez-Wing, J. Ascencio and M. J. Yacaman, *Phys. Status Solidi B*, 2002, **230**, 363.
29 M. Brust, M. Walker, D. Bethell, D. J. Schiffrin and R. Whyman, *J. Chem. Soc., Chem. Commun.*, 1994, 801.
30 P. Khanal and E. R. Zubarev, *Angew. Chem., Int. Ed.*, 2007, **46**, 2195.
31 L. Zhang, H. Y. Si and H. L. Zhang, *J. Mater. Chem.*, 2008, **18**, 2660.
32 N. S. John, G. Raina, A. Sharma and G. U. Kulkarni, *J. Chem. Phys.*, 2010, **133**, 094704.
33 A. Sweetman, P. Sharp, A. Stannard, S. Gangopadhyay and P. Moriarty, *Proc. SPIE–Int. Soc. Opt. Eng.*, 2008, **7041**, 704102.
34 A. Sweetman, PhD thesis, University of Nottingham, 2010.
35 A. Stannard, PhD thesis, University of Nottingham, 2009.
36 J. M. Topple, S. A. Burke, S. Fostner and P. Grutter, *Phys. Rev. B: Condens. Matter Mater. Phys.*, 2009, **79**, 205414.
37 S. A. Burke, J. M. Topple and P. Grutter, *J. Phys.: Condens. Matter*, 2009, **21**, 423101.
38 D. Kafer, C. Woll and G. Witte, *Appl. Phys. A: Mater. Sci. Process.*, 2009, **95**, 273.
39 J. A. Hayton, E. Pauliac-Vaujour and P. Moriarty, *Nano*, 2007, **2**, 361.
40 C. P. Martin, M. O. Blunt, E. Pauliac-Vaujour, A. Stannard, P. Moriarty, I. Vancea and U. Thiele, *Phys. Rev. Lett.*, 2007, **99**, 116103.

This journal is © The Royal Society of Chemistry 2011

*J. Mater. Chem.*, 2011, **21**, 16983–16989 | 16989